

The Limits of Cosmic Shear

Thomas D. Kitching^{1*}, Justin Alsing^{2,3}, Alan F. Heavens², Raul Jimenez^{4,5},
 Jason D. McEwen¹, Licia Verde^{4,5}

¹*Mullard Space Science Laboratory, University College London, Holmbury St Mary, Dorking, Surrey RH5 6NT, UK*

²*ICIC, Astrophysics, Imperial College, Blackett Laboratory, Prince Consort Road, London SW7 2AZ, UK*

³*Center for Computational Astrophysics, 160 5th Ave, New York, NY 10010, USA*

³*ICC, University of Barcelona, IEEC-UB, Martí Franques, 1, E08028 Barcelona, Spain*

⁴*ICREA, Pg. Lluís Companys 23, 08010 Barcelona, Spain*

ABSTRACT

In this paper we discuss the commonly-used approximations for two-point cosmic shear statistics. We discuss the four most prominent assumptions in this statistic: the flat-sky, tomographic, Limber and configuration-space approximations, that the vast majority of cosmic shear results to date have used simultaneously. Of these approximations we find that the flat-sky approximation suppresses power by $\gtrsim 1\%$ on scales of $\ell \lesssim 100$ and the standard Limber approximation implementation enhances power by $\gtrsim 5\%$ on scales $\ell \lesssim 100$; in doing so we find an ℓ -dependent factor that has been neglected in analyses to date. To investigate the impact of these approximations we reanalyse the CFHTLenS 2D correlation function results. When using all approximations we reproduce the result that measurements of the matter power spectrum amplitude are in tension with measurements from the CMB Planck data: where a conditional value of $\sigma_8 = 0.789 \pm 0.015$ is found from CFHTLenS and $\sigma_8 = 0.830 \pm 0.015$ from Planck. When we do not use the Limber and flat-sky approximations we find a conditional value of $\sigma_8 = 0.801 \pm 0.016$ from the CFHTLenS data, significantly reducing the tension between Planck CMB results and lensing results from CFHTLenS. When including the additional effect of expected photometric redshift biases we find $\sigma_8 = 0.839 \pm 0.017$ which is consistent with Planck. We also discuss the impact on CMB lensing. For Euclid, LSST, and WFIRST and any current or future survey none of these approximations should be used.

Key words: Cosmology: theory – large-scale structure of Universe

1 INTRODUCTION

Weak lensing is the phenomenon whereby the images of distant galaxies are distorted by the effect of gravitational potentials caused by matter perturbations along the line-of-sight. This gravitational lensing effect induces a small change in the ellipticity¹ of a galaxy’s image known as shear. The shear caused by the large-scale structure of the Universe is known as ‘cosmic shear’. The mean of the complex cosmic shear field is zero but its 2-point correlation function or power spectrum contains cosmological information; cosmic shear is also used as a synonym for this statistic. This statistic is a particularly sensitive probe of dark energy because it measures the power spectrum of matter overdensity perturbations across large portions of the expansion history of the Universe. Because of this there are several on-going

wide-field surveys that attempt to measure this effect, for example CFHTLenS (Heymans et al., 2012), DES (The DES Collaboration et al., 2015), DLS (Jee et al., 2015), KiDS (Kuijken et al., 2015), and HyperSuprimeCam; as well as several more planned surveys, for example *Euclid*² (Lau-reijs et al., 2011), LSST (LSST Science Collaboration et al., 2009), and *WFIRST* (Spergel et al., 2015), that have the measurement of this statistic as one of their primary science goals.

In practice there are several ways in which the cosmic shear 2-point statistic can be computed that can be broadly categorised into real/configuration-space measurements as a function of celestial angle known as correlation functions, and angular spherical-harmonic/Fourier-space measurements known as power spectra. Furthermore these statistics can be computed in a series of redshift bins, to capture the geometry of the three-dimensional shear

* t.kitching@ucl.ac.uk

¹ Third flattening, or third eccentricity.

² <http://euclid-ec.org>

field, an approach known as ‘tomography’; or a spherical-Bessel/Fourier-space measurement in the radial direction known as ‘three-dimensional’ cosmic shear (Heavens, 2003, Castro et al., 2005, Kitching et al. 2007).

In this paper we present each of the primary approximations in cosmic shear statistics and explicitly link all of the currently used statistics together into a general schema. In doing so we also present a general three-dimensional spherical-radial statistic which is the redshift-space equivalent of a spherical-Bessel analysis. We discuss various approximations and a data compression, namely: flat-sky, Limber, tomography and Hankel transformations. The flat-sky assumption assumes that the cosmic shear analysis is done on a locally flat tangent plane on the sky. The tomographic data compression, presented in Hu (1999), is a lossy binning of the cosmic shear signal into several redshift bins and is an approach used by *all* cosmic shear studies (see Kilbinger, 2015 for a review) except those that use a spherical-Bessel representation (e.g. Kitching et al. 2014), for both theoretical studies and data analysis. In Kitching, Heavens, Miller (2011) and Kitching et al. (2014) it was shown how to derive the tomographic case from a more general spherical-Bessel representation of the shear field. The Limber approximation links angular and radial wavenumbers together via a co-moving distance relation. This was first discussed in Kaiser (1998) in the context of cosmic shear and has been investigated in Simon (2007) and Kitching, Heavens, Miller (2011) in cosmic shear studies, but in the majority of theoretical studies and data analyses it is an axiomatic assumption (i.e. an unquestioned and untested assumption at the beginning of the analysis). There is a particularly clear illustration of the Limber approximation in LoVerde & Afshordi (2008) that we discuss in this paper.

Most of the approximations we investigate are used simultaneously and in combination. Notably *all* the primary cosmological results from all of the wide-field surveys use a flat-sky, tomographic, Limber-approximated correlation function analysis, i.e., Heymans et al. (2013) for CFHTLenS; The DES Collaboration et al., (2015) for DES; Jee et al. (2015) for DLS and Hildebrandt et al. (2016) for KiDS. Notable exceptions include Pen et al. (2002), Brown et al. (2003), Heymans et al. (2005), Kohlinger et al. (2016), Alsing et al. (2016b), and the **PolSpice** measurements in The DES Collaboration et al., (2015), all whom used Fourier-space measurements in angle, with the flat-sky, tomographic and Limber approximations. In Kitching et al. (2007) and Kitching et al. (2014) a flat-sky spherical-Bessel analysis was used without the tomographic or Limber approximations.

This paper is presented in the following manner. In Section 2 we review the cosmic shear formalism starting with the spherical-Bessel representation and then present the spherical-radial and correlation function representations. In Section 3 we discuss the flat-sky, tomographic and Limber approximations and present a general schema for linking these statistics and approximations. We discuss the implications of this for current results in Section 4. We discuss conclusions in Section 5.

2 COSMIC SHEAR METHODS

We begin by introducing several versions of the two-point cosmic shear statistic that treat the data, and represent the underlying three-dimensional shear field, in different ways. The first of these is the spherical-Bessel representation that has been described in detail in Heavens (2003); Castro, Heavens, Kitching (2005); Heavens, Kitching, Taylor, (2006); Kitching (2007); Kitching, Taylor, Heavens, (2008); Kitching, Heavens, Miller (2011); Kitching et al. (2007); Kitching et al. (2014), the second is the presentation of a spherical-radial representation of which the commonly used tomographic statistic is a simple approximation. We then discuss real/configuration-space representations.

2.1 The Spherical-Bessel Representation

The cosmic shear field has spin-weight 2, and we can perform a spherical-Bessel transform to obtain

$$\gamma_\ell^m(k) = \sum_g \gamma_g(r_g, \theta_g) j_\ell(kr_g) {}_2Y_\ell^m(\theta_g) \quad (1)$$

where the sum is over all galaxies g at three-dimensional co-moving coordinates (r_g, θ_g) , k is a radial wavenumber and ℓ is an angular wavenumber. The $j(kr_g)$ are spherical Bessel functions. The ${}_2Y_\ell^m(\theta_g)$ are spin-weight 2 spherical harmonics. Such a sum can be used to construct the data vector for a spherical-Bessel analysis of weak lensing data, which is then compared with the following theoretical covariance, as described in Kitching et al. (2014). When applying this sum to data these transformed coefficients can be manipulated to extract the pure E and B-mode signals (where cosmic shear is only expected to produce an E-mode signal), and remove any multiplicative measurement biases (where the measured γ_g is related to the true γ_g^T via some linear relation $\gamma_g = (1 + m)\gamma^T$, where m is an estimated bias parameter) as described in Kitching et al. (2014). The sum over galaxies is an estimator for a continuous integral over angle and radius, where there is an additional shot-noise contribution to the covariance, due to having a finite number of galaxies at discrete points (see Heavens, 2003).

The mean of equation (1) is zero, but the covariance of the transform coefficients is non-zero. Assuming isotropy the covariance of the harmonic coefficients – known as the power spectrum – can be written as

$$\langle \gamma_\ell^m(k) \gamma_{\ell'}^{m'*}(k') \rangle = C_\ell^{SB}(k, k') \delta_{\ell\ell'} \delta_{mm'}. \quad (2)$$

Using the notation of Kitching, Heavens, Miller (2011), we can write down the theoretical expectation value of the power spectrum for given a cosmology

$$C_\ell^{SB}(k, k') = |D_\ell|^2 \mathcal{A}^2 \int \frac{d\tilde{k}}{\tilde{k}^2} G_\ell^{SB}(k, \tilde{k}) G_\ell^{SB}(k', \tilde{k}), \quad (3)$$

where the pre-factor $\mathcal{A} = 3\Omega_M H_0^2/(2\pi c^2)$ (where H_0 is the current value of the Hubble parameter, Ω_M is the ratio of the total matter density to the critical density, and c is the speed of light in a vacuum). The variable $|D_\ell| = \sqrt{(\ell + 2)!/(\ell - 2)!}$ in the spherical case (see Castro et al., 2005; and Leistedt et al., 2015), this is approximated by $|D_\ell| = \ell^2$ in the flat-sky case (see section 3.1). The G matrix is given by

$$G_\ell^{SB}(k, \tilde{k}) = \int dz_p j_\ell(kr(z_p)) n(z_p)$$

$$\times \int dz' p(z'|z_p) U_\ell(r[z'], \tilde{k}), \quad (4)$$

where $n(z_p)dz_p$ is the number of galaxies in a spherical shell of radius z_p and thickness dz_p , and $p(z'|z_p)$ is the probability of a galaxy with photometric redshift z_p having a true redshift z' . The U matrix is given by

$$U_\ell(r[z], k) = \int_0^{r[z]} dr' \frac{F_K(r, r')}{a(r')} j_\ell(kr') P^{1/2}(k, r'), \quad (5)$$

where $P(k, r[z])$ is the matter power spectrum at comoving distance $r[z]$ and radial wavenumber k . The comoving distance r is used to express the time-dependence of the power spectrum; we could equally use t as a label, or $r(t)$. $F_K = S_K(r-r')/S_K(r)/S_K(r')$ is the ‘lensing kernel’ where $S_K(r) = \sinh(r)$, $r, \sin(r)$ for cosmologies with spatial curvature $K = -1, 0, 1$, and $a(r)$ is the dimensionless scale factor at the cosmic time related to the look-back time at comoving distance r .

2.2 The Spherical-Radial Representation

A different way to represent the three-dimensional shear field is to make a Fourier-like decomposition in angular wavenumber but *not* in the radial direction. This decomposition is the following

$$\gamma_\ell^m(z) = \sum_{g \in z} \gamma_g(r_g, \theta_g) {}_2Y_\ell^m(\theta_g) \quad (6)$$

which is still a three-dimensional representation of the data, except that it excludes the radial Bessel transform. The sum in this case is over all galaxies that have a redshift z . We refer to this as the ‘spherical-radial’ transform (as opposed to a spherical-Bessel transform).

Again the mean of this representation is zero, but the covariance is non-zero. Using the notation above, we can write down the theoretical expectation value of the power spectrum given a cosmology

$$C_\ell^{SR}(z, z') = |D_\ell|^2 \mathcal{A}^2 \int \frac{dk}{k^2} G_\ell^{SR}(z, k) G_\ell^{SR}(z', k), \quad (7)$$

where in this case the G^{SR} matrix is given by

$$G_\ell^{SR}(z, k) = \int dz_p W^{SR}(z, z_p) n(z_p) \times \int dz' p(z'|z_p) U_\ell(r[z'], k), \quad (8)$$

where $W(z, z_p)$ is a redshift-dependent weight function that defines the ‘bin-width’ in redshift over which the statistic is defined for redshift z . The U matrices are the same as in equation (5). In the case that $W^{SR}(z, z_p) = \delta^D(z - z_p)$ this covariance is still a complete representation of the shear field when z and z' span $[0, \infty)$.

2.3 The Configuration-Space Representation

As an alternative to performing a cosmic shear statistic in Fourier/Bessel space the analysis can be done in real/angular/configuration space, where instead of an angular wavenumber an angle on the celestial sphere is used θ

as the dependent variable. Such statistics are readily computed from data by summing over pairs of galaxies (see e.g. Kilbinger, 2015). From theory these are related to the cosmic shear power spectra through a Hankel transform that results in two correlation functions

$$\begin{aligned} \xi_+(\theta, z, z') &= \frac{1}{2\pi} \int d\ell \ell J_0(\ell\theta) C_\ell^{SR}(z, z') \\ \xi_-(\theta, z, z') &= \frac{1}{2\pi} \int d\ell \ell J_4(\ell\theta) C_\ell^{SR}(z, z'). \end{aligned} \quad (9)$$

This assumes a flat-sky approximation. In Castro et al. (2005) spherical-sky formulae are provided for similar transforms but these are not currently in use. These can be performed either in three-dimensions (a flat-sky plus a radial line), as we have used here, or on tomographically binned data. In this case the power spectra in the integrals are a sum of both E-mode and B-mode components. An inverse-Hankel transform can also be defined e.g., $C_\ell^{SR}(z, z') = \int d\theta \ell J_0(\ell\theta) \xi_+(\theta, z, z')$ but since this formally requires an integration over *all* angles it is not well-defined in the flat-sky case.

In the cosmic shear representations that are based on spherical harmonic transforms the angular wavenumbers can be related to celestial angular separations through $\theta = \pi/\ell$. However after performing the Hankel transformation the relationship between the angle θ in equations (9) is more complicated. To investigate this relation we plot in Figure 1 the Bessel function amplitudes in equation (9) as a function of ℓ -mode and θ , for the ξ_+ and ξ_- functions. It is clear from these figures that every angle samples from all ℓ -modes but weighted in a different way. To estimate which ℓ -modes contribute to the Hankel transform integrals we compute the following over θ

$$\begin{aligned} \mathcal{W}_+(\ell, z, z') &= \int_{\theta_{\min}}^{\theta_{\max}} d\theta [\ell J_0(\ell\theta) C_\ell^{SR}(z, z')] \\ \mathcal{W}_-(\ell, z, z') &= \int_{\theta_{\min}}^{\theta_{\max}} d\theta [\ell J_0(\ell\theta) C_\ell^{SR}(z, z')]. \end{aligned} \quad (10)$$

These are the weight functions in ℓ -mode, integrated over all angles, that are applicable for analyses that require a sum over angle (such as a likelihood function). We use $\theta_{\max} = 100$ arcminutes, and vary θ_{\min} and show these functions in Figure 1. To compute the maximum ℓ -mode to minimum θ relationship we compute the cumulative functions

$$\left(\frac{1}{A}\right) \int_2^{\ell_{\max}} d\ell |\mathcal{W}_+(\ell, r, r')| = f \leq 1, \quad (11)$$

that we calculate as a discrete sum, where $A = \int_2^\infty d\ell |\mathcal{W}_+(\ell, r, r')|$. These functions only converge to machine precision at $\ell_{\max} \rightarrow \infty$ so in practice a tolerance needs to be defined f where it is considered that most of the information is captured. We set this to $f = 0.995$, i.e. 99.5% of the integral content is captured by this limit, we find that larger than this and numerical errors become dominant. We plot this derived ℓ_{\max} in Figure 1, and find that the link between ℓ_{\max} and θ_{\min} is well-approximated by the following scaling functions

$$\begin{aligned} \xi_+ : \log_{10}[\ell_{\max}] &= -0.14 \log_{10}(\theta_{\min}/\text{arcmin}) + 4.06 \\ \xi_- : \log_{10}[\ell_{\max}] &= -0.19 \log_{10}(\theta_{\min}/\text{arcmin}) + 4.49. \end{aligned} \quad (12)$$

We find that the ξ_- statistic is much more sensitive to high-

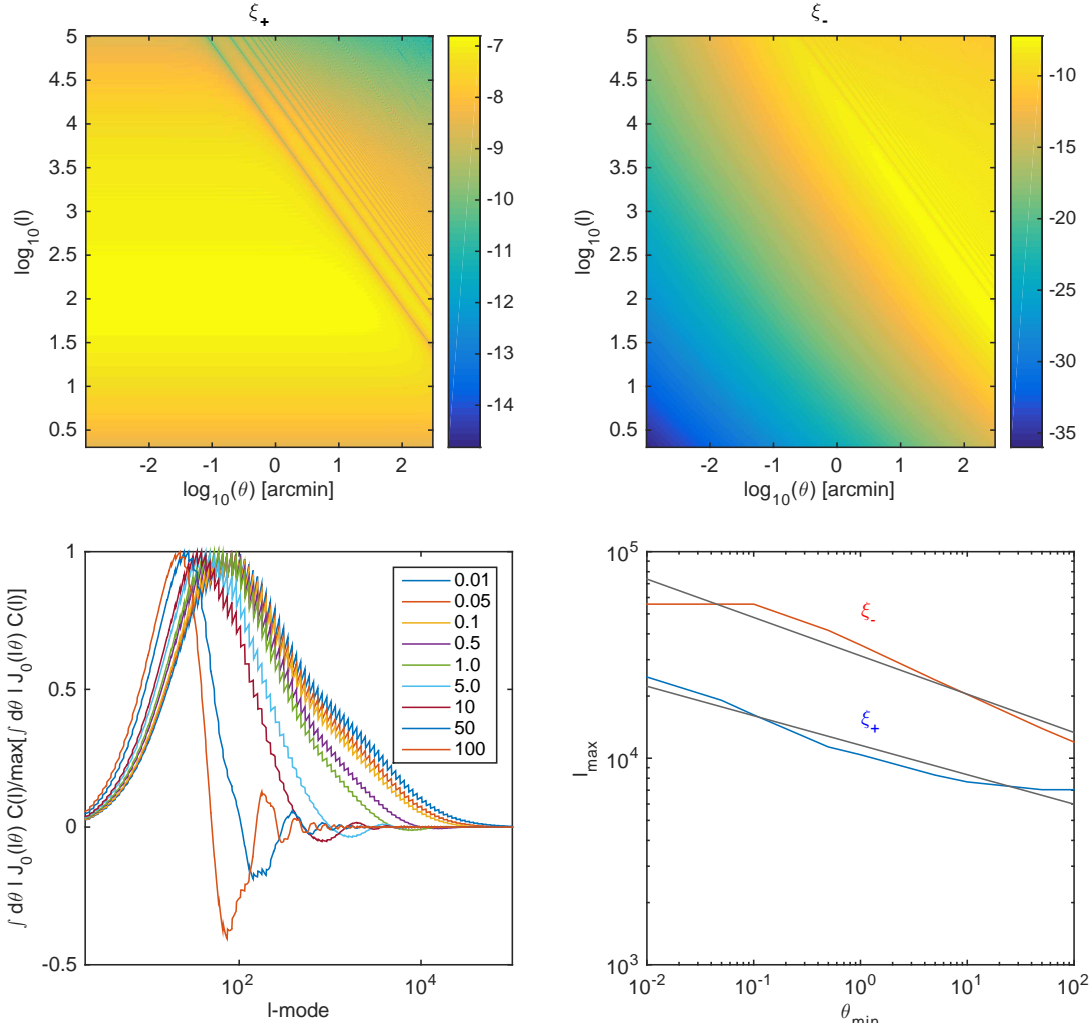


Figure 1. The top panels show the functions $\ell J_0(\ell\theta) C_\ell^{SR}(z, z)$ (left-hand panel) and $\ell J_4(\ell\theta) C_\ell^{SR}(z, z)$ (right-hand panel) for an auto-correlation cosmic shear power spectrum $C_\ell^{SR}(z, z)$ evaluated at a redshift of zero; although we find results in this Figure are insensitive to this assumption. The colour scales denote the logarithm (base-10) of the magnitude of the functions that correspond to the ξ_+ and ξ_- Hankel transforms respectively. The lower left panel shows the normalised integral $\int d\theta \ell J_0(\ell\theta) C_\ell^{SR}(z, z)$ over θ to show the integrated weighting of $\int d\theta \xi_\pm(\theta)$ as a function of ℓ -modes for a variety of angular ranges $\theta_{\min} \leq \theta \leq 100$. The different labelled colours in this plot show different θ_{\min} in arcminutes. The lower right-hand panel shows the ℓ_{\max} where these integrals converge as a function of θ_{\min} for the ξ_+ (blue) and ξ_- (red) Hankel transforms. The fitted functions in equation (12) are shown in grey.

ℓ modes than ξ_+ . For typical minimum angles used in data analysis of $\theta_{\min} \sim 0.1$ arcminutes we find that the maximum wavenumber probed is approximately $\ell_{\max} \sim 5 \times 10^4$ for the ξ_+ statistic.

To estimate correlation functions from data formally requires summing over all galaxy pairs separated by arbitrary angles. In practice such a sum is difficult, therefore several ways of filtering the ‘raw’ correlation function measurement (equation 9) have been proposed that result in finite angular limits, for example Top-hat statistics, Map statistics (e.g. Munshi et al., 2004) and COSEBIs (e.g. Schneider et al., 2010). These are well summarised and reviewed in Kilbinger (2015).

3 COSMIC SHEAR APPROXIMATIONS

We will now investigate the impact of several approximations that are commonly used in cosmic shear studies. We will address the flat-sky, tomographic and Limber approximations, but will not discuss source-source clustering (Schneider et al. 2002), source-lens clustering (Bernardeau 1998, Hamana et al. 2002), the Born approximation (Cooray & Hu, 2002), higher-order power spectrum terms (Krause & Hirata, 2010), or unequal-time correlations (Kitching & Heavens, 2016); all of which are expected to have an effect for future surveys (Euclid, LSST and WFIRST) but not for current surveys.

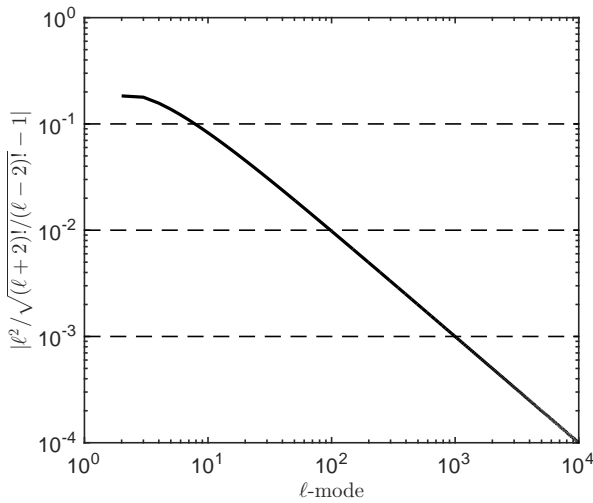


Figure 2. The ratio of the cosmic shear power spectrum in spherical-sky case compared to the flat-sky case. The solid line shows the ratio, and the dashed lines demarcate decadal values on the y -axis to help guide the reader. The y -axis label shows the two pre-factors that occur in the spherical-sky and flat-sky cases $\sqrt{(\ell+2)!(\ell-2)!}$ and ℓ^2 respectively.

3.1 The Flat-Sky Approximation

The flat-sky approximation assumes that the angular extent of the observational field is small and hence the geometry of the angular component is assumed to be planar (i.e., Euclidean). In this case a planar transform is done instead of a spherical transform in equations (1) and (6) which results in an exponential term $\exp(i\ell\theta)$ instead of the spin spherical harmonics.

In the case of computing the transform coefficients from data, equations (1) and (6), this results in a different sum over galaxies. In the computation of data vectors the weighting as a function of ℓ mode is therefore significantly different (see e.g. Hu, 2000).

However in the computation of the theoretical covariances, due to the similar orthogonality relations between both the spherical harmonic and the exponential functions, equations (3) and (7), this only results in a simple change to the pre-factor $|D_\ell|$ from $|D_\ell| = \sqrt{(\ell+2)!(\ell-2)!} \rightarrow \ell^2$. This is a result of the different ways that the spin raising and lowering operators (that relate the shear field to the gravitational potential field) act on the spin spherical harmonics and the exponential functions; see Appendix A of Castro et al. (2005). The impact of this approximation on the amplitude of the cosmic shear covariance can then very simply be computed, and we show this ratio in Figure 2.

It can be seen that for $\ell \lesssim 10$ there is a more than 10% change which reduces to $\lesssim 1\%$ for $\ell \gtrsim 100$. In order to assess the impact of this approximation we refer to Massey et al., (2013) where a requirement on the multiplicative changes in the cosmic shear power spectrum caused by systematic effects (which is the case here) to be less than 4×10^{-3} in total for a *Euclid*-like cosmic shear experiment, which is relaxed to $\sim 4 \times 10^{-2}$ for a KiDS or DES-like survey (see e.g. Kitching et al., 2008). These requirements suggests that *Euclid*-like surveys should not use this approximation because

even at $\ell \lesssim 1000$ a quarter of the total allowance for all systematic effects would be used by the flat-sky approximation. For current KiDS and DES-like surveys this approximation accounts for 10% of the total systematic budget at $\ell \lesssim 500$. These results are applicable for the computation of the theoretical covariances (i.e. power spectra), but the data vector computation is also affected (see e.g. Hu, 2000).

3.2 Tomographic Data Compression

The tomographic approximation involves the computation of projected two-dimensional power spectra in a series of redshift bins including the inter-bin (auto-correlation) and intra-bin (cross-correlation) power spectra. This is not an approximation in itself, but it is a lossy data compression.

We look at the effect of this binning by first relating the spherical-Bessel and spherical-radial transforms together. As shown in Kitching et al. (2014) the shear transform coefficients, from our equations (1) and (6), can be related through a radial transform

$$\gamma_\ell^m(z_1) = \int dr W^{SR}[z_1, z(r)] \int dk j_\ell(kr) \gamma_\ell^m(k) \quad (13)$$

where the weight function is the same one that appears in equation (8), where the integrand of comoving distance r is related to a redshift $z(r)$, and describes the bins as a function of redshift. When referring to tomography we use numbered redshifts e.g. z_1 and z_2 , rather than z and z' . We note that only in the case that the weight function is a delta-function is this a full description of the three-dimensional shear field. In the case that the bin-width is finite we will refer to this as a ‘tomographic’ representation of the shear field.

By taking the covariance of equation (13) the two power spectra can be related through

$$C_\ell^{SR}(z_1, z_2) = \int dk dk' dr' dr'' W^{SR}[z_1, z(r')] W^{SR}[z_2, z(r'')] j_\ell(kr') j_\ell(k'r'') C_\ell^{SB}(k, k'). \quad (14)$$

This transformation from spherical-Bessel to spherical-radial (tomographic) representations can be performed for any integrable weight function W^{SR} ; this is also discussed in Castro et al. (2005).

The reverse transform can also be computed, but *only* in the case that the weight function is a delta-function in redshift. In this specific case the reverse transform is

$$C_\ell^{SB}(k, k') = \int dz dz' j_\ell(kr[z]) j_\ell(k'r[z']) C_\ell^{SR}(z_1, z_2), \quad (15)$$

where the integration over redshift is formally over $0 \leq z < \infty$.

It has been shown (e.g. Bridle & King, 2007) that only 10 – 20 redshift bins are required in order for the cosmic shear power spectrum to be sufficiently sampled in redshift to extract the majority of cosmological information. This is because the lensing kernel is a relatively broad function in redshift space. This is applicable when describing the shear field using the spherical-radial representation, with the caveats that such current studies of the convergence of this approximation have assumed the flat-sky and Limber approximations (that we discuss in the next Section).

3.3 The Limber Approximation

The Limber (Limber, 1953) approximation was first introduced in Kaiser (1998) for cosmic shear studies as a method for rendering the calculations more tractable and understandable, and has subsequently been used in the majority of the cosmic shear studies, both in methodological development and in applications to data. In Simon (2007) configuration-space (real variable in angle) measurements of galaxy clustering were considered with a conclusion that for angular separations of $\gtrsim 10$ arcminutes there is more than a 10% bias in correlation function measurements.

In LoVerde & Afshordi (2008) a particularly clear explanation of the approximation was provided. This assumed that the matter power spectrum was not evolving, i.e. it can be expressed as a function of k -mode only $P(k)$ (LoVerde & Afshordi, 2008; equation 5). Unfortunately the LoVerde & Afshordi (2008) approximation is not directly appropriate at all orders for the cosmic shear setting where the shear field is an integrated effect over an evolving matter power spectrum; an assumption that we address in Appendix A. In Kitching, Heavens, Miller (2011) the effect of the Limber approximation on cosmic shear was investigated using the LoVerde & Afshordi (2008) approximation, and an effect on the expected error bars of cosmological parameters was predicted.

If the Limber approximation is assumed then using the Kaiser (1998) and LoVerde & Afshordi (2008) approximation the spherical-radial representation of the cosmic shear field can be written as

$$C_\ell^{SR}(z_1, z_2) \simeq |D_\ell|^2 \mathcal{A}^2 \int \frac{dk}{k^2} P(k, \nu/k) f(z_1, \nu/k) f(z_2, \nu/k) \quad (16)$$

where the variable $\nu = \ell + 1/2$. In Appendix A we show that this is indeed the first order approximation to the cosmic shear power spectrum despite the assumption of a constant matter power spectrum, however the expansion of this to higher order does not result in a convergence towards the unapproximated case if redshift-independent limits in angular wavenumber are assumed. The kernel functions are

$$f(z_1, \nu/k) = \left(\frac{\pi}{2\nu k^2} \right) \int dz' dz_p n(z_p) p(z'|z_p) W^{SR}(z_1, z_p) \frac{F_K(r[z'], \nu/k)}{a(\nu/k)}. \quad (17)$$

This expression is not entirely in the same form as commonly used in the cosmic shear literature (e.g. Hu, 1999; Joachimi & Bridle, 2009; Heymans et al. 2013), where the standard form is to use an inner integral over r instead of k -mode. As shown in Appendix A when doing this we find that the Limber-approximated power is given by

$$C_\ell^{SR}(z_1, z_2) \simeq |D_\ell|^2 \mathcal{A}^2 \left(\frac{1}{\nu^4} \right) \int dr q(r_1, r) q(r_2, r) P(\nu/r, r), \quad (18)$$

where

$$q(r_1, r) = \frac{r}{a(r)} \int dz_p dz' n(z_p) p(z|z_p) W^{SR}(z_1, z_p) \left(\frac{r(z') - r}{r'} \right) \quad (19)$$

where we have expanded the function F_K , and we have assumed here a flat-geometry ($K = 0$). This is the stan-

dard form for the cosmic shear power spectrum (see e.g. Hu, 1999; Joachimi & Bridle, 2009), except that there is an ℓ -dependent pre-factor

$$T_\ell = \frac{|D_\ell|^2}{\nu^4} = \frac{(\ell + 2)(\ell + 1)\ell(\ell - 1)}{(\ell + 0.5)^4}. \quad (20)$$

In the standard derivation there are two assumptions that remove this pre-factor. These assumptions are: the flat-sky approximation whereby $|D_\ell|^2 = \ell^4$, and the approximation $\nu = \ell$. In this case $T_\ell = 1$ and the standard result is recovered, where there is no ℓ -mode weighting. However these approximations can have a large impact on the amplitude of the power spectrum at $\ell \lesssim 100$ as we investigate in this paper. To recover the correct ℓ -mode scaling from a standard cosmic shear analysis one should multiply a standard Limber-approximated power spectrum by T_ℓ . In the flat-sky limit $T_\ell = \ell^4/(\ell + 0.5)^4$. In Figure 3 we show the change in the power spectrum amplitude as a function of ℓ -mode caused by these effects. Relative to the full case the Limber, $T_\ell = 1$ and flat-sky approximations act to enhance the power on large-scales. The flat sky approximation itself acts to decrease the power. Therefore the largest difference is between the flat-sky non-Limber case, and the Limber, $T_\ell = 1$ and flat-sky approximated case; this is the relevant case for current correlation function measurements that use a flat-sky Hankel transform of the power spectrum. We find that this difference is $\gtrsim 5\%$ on scales of $\ell \lesssim 100$. In Section 3.5 we will investigate the impact of these effects on cosmological parameter estimation.

Up to first order the Limber approximation can be summarised by comparing equation (7) with equation (16) as a replacement of Bessel functions with scaled delta functions inside the integrals

$$k^{1/2} j_\ell(kr) \simeq \sqrt{\frac{\pi}{2\ell + 1}} \delta^D(\ell + 1/2 - kr) \quad (21)$$

as shown in Leistedt et al. (2015). This expression shows how the Limber approximation acts to link the angular and radial modes through the relation $\ell = kr[z] - 1/2$, that we also derive in Appendix A, which has an important effect on the computation of cosmic shear power spectra.

Finally we also note that the derivative of a Limber-approximated power spectrum is not equal to the Limber-approximation of the derivative. This can be seen relatively straightforwardly by considering the LoVerde & Afshordi (2008) approximation, equation (25), which means that statistics that use Limber-approximated quadratic estimators to measure the cosmic shear power spectrum are not accurate (e.g., Kohlinger et al., 2015).

3.4 A Schema of Cosmic Shear Statistics

Each of the cosmic shear representations and approximations can be linked in a series of transformations that relate one to the other. For example in Kitching, Heavens, Miller (2011) and Kitching et al. (2014) we show how to relate the spherical-Bessel to the tomographic representation (we also show this in Appendix A). In this paper we show how to transform from the spherical-Bessel to spherical-radial cases. The flat-sky and configuration-space approximations are well-known as we have discussed.

We show how all of these are linked together in Figure 4

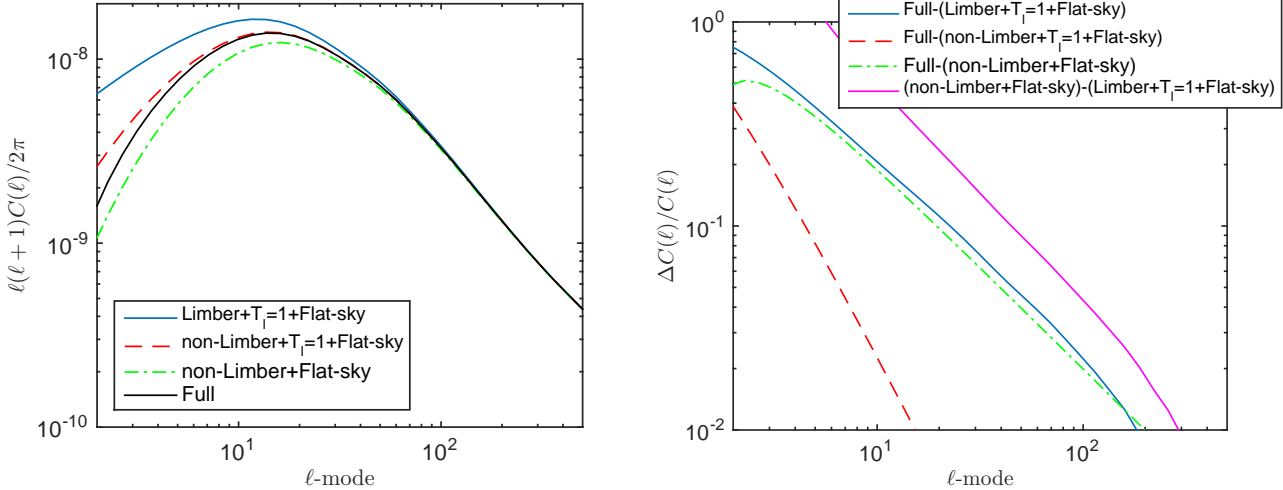


Figure 3. Left panel: 2D cosmic shear power spectra, using CFHTLenS number density. We show the full spherical-sky non-Limber approximated case (black line), the non-Limber approximated flat-sky case (green dot-dashed line), the non-Limber approximated flat-sky case assuming $T_\ell = 1$ (red dashed line), and the Limber approximated flat-sky case assuming $T_\ell = 1$ (blue line). Right panel: The ratio of the cosmic shear power spectrum in spherical-sky non-Limber approximated case compared to power spectra that include the Limber approximation, the effect of $T_\ell = 1$ (equation 20), and the flat-sky approximation.

where we relate each of the cosmic shear statistics together via the network of approximations that can be employed. In this Figure arrows indicate the direction that the transform takes the statistic, where only one such case is reversible³ (the three-dimensional radial transform). We also link the points at which estimators from data are linked to the theoretical statistics, and highlight those statistics that have been applied to data. This provides a visual way to understand what transformation need to be made to interpret any given cosmic shear data analysis, where any statistical assumptions have been made, and how a given observation can be translated into another.

3.5 Application to data

We now investigate the impact of the flat sky and Limber approximations on cosmological parameter inference from current cosmic shear data. In Figure 5 we show the CFHTLenS 2D correlation function measurement⁴. For comparison are the predicted correlation functions for a *Planck* (Planck Collaboration et al., 2015) maximum likelihood cosmology⁵ in the Limber-approximated and non-Limber approximated cases. The non-Limber predicted correlation functions were derived by computing the full $C_\ell^{SR}(z_1, z_1)$ over the ranges $0 \leq k \leq 100 h \text{Mpc}^{-1}$ and $0 \leq z \leq 3$ in the (k, z) plane, with z_1 equal to the mean redshift of the CFHTLenS $n(z)$ distribution, and then performing the Hankel transform. However

³ By reversible we mean that it can be performed in either direction, without loss of information.

⁴ Using the publicly available data here <http://www.cfhtlens.org>.

⁵ Where the dimensionless matter density is $\Omega_M = 0.3$, the Hubble parameter is $h = 0.67$, the dimensionless baryon density is $\Omega_B = 0.049$, the dark energy equation of state is $w = -1$, and the scalar spectral index is $n_s = 0.96$.

we note that the Hankel transform itself assumes a flat-sky approximation (equation 9). For all calculations we used the CFHTLenS number density distributions given in Kilbinger et al. (2013).

It can be seen that the ξ_+ function is affected more by the approximations, as may be expected because it is sensitive to lower ℓ -modes, see Section 2.3, and that the non-Limber-approximated predictions are a better fit to data (even in this case that the data points are correlated, and so ‘ χ -by-eye’ should be done with caution). Using the full covariance matrices from CFHTLenS we find that the reduced χ^2 values (with 42 degrees of freedom) for a maximum likelihood *Planck* cosmology are: 1.93 and 1.03 for ξ_+ and ξ_- using the Limber approximation; 1.05 and 1.02 for ξ_+ and ξ_- using the full case (the reduced χ^2 is expected to be 1 ± 0.15 for ξ_+ and ξ_- given the number of data points in the sample).

In Figure 6 we show a fit to the data when varying σ_8 , assuming all other parameters fixed at the *Planck* maximum likelihood values. We perform a χ^2 test on the data

$$\chi^2 = \sum_{\theta} \sum_{\theta'} \left(\begin{array}{c} \xi_+^T(\theta) - \xi_+^D(\theta) \\ \xi_-^T(\theta) - \xi_-^D(\theta) \end{array} \right) \left(\begin{array}{cc} C_{++} & C_{+-} \\ C_{-+} & C_{--} \end{array} \right)^{-1} \left(\begin{array}{c} \xi_+^T(\theta') - \xi_+^D(\theta') \\ \xi_-^T(\theta') - \xi_-^D(\theta') \end{array} \right)^T \quad (22)$$

where the sum is over all angular values, $C_{++/-/+/-/-}$ are the covariance matrices of the measurements⁶, and $\xi_{+/-}^T(\theta)$ and $\xi_{+/-}^D(\theta)$ are the theory and data vectors of the correlation functions respectively; this is the same as the ex-

⁶ Using the publicly available estimated covariance matrices here <http://www.cfhtlens.org>

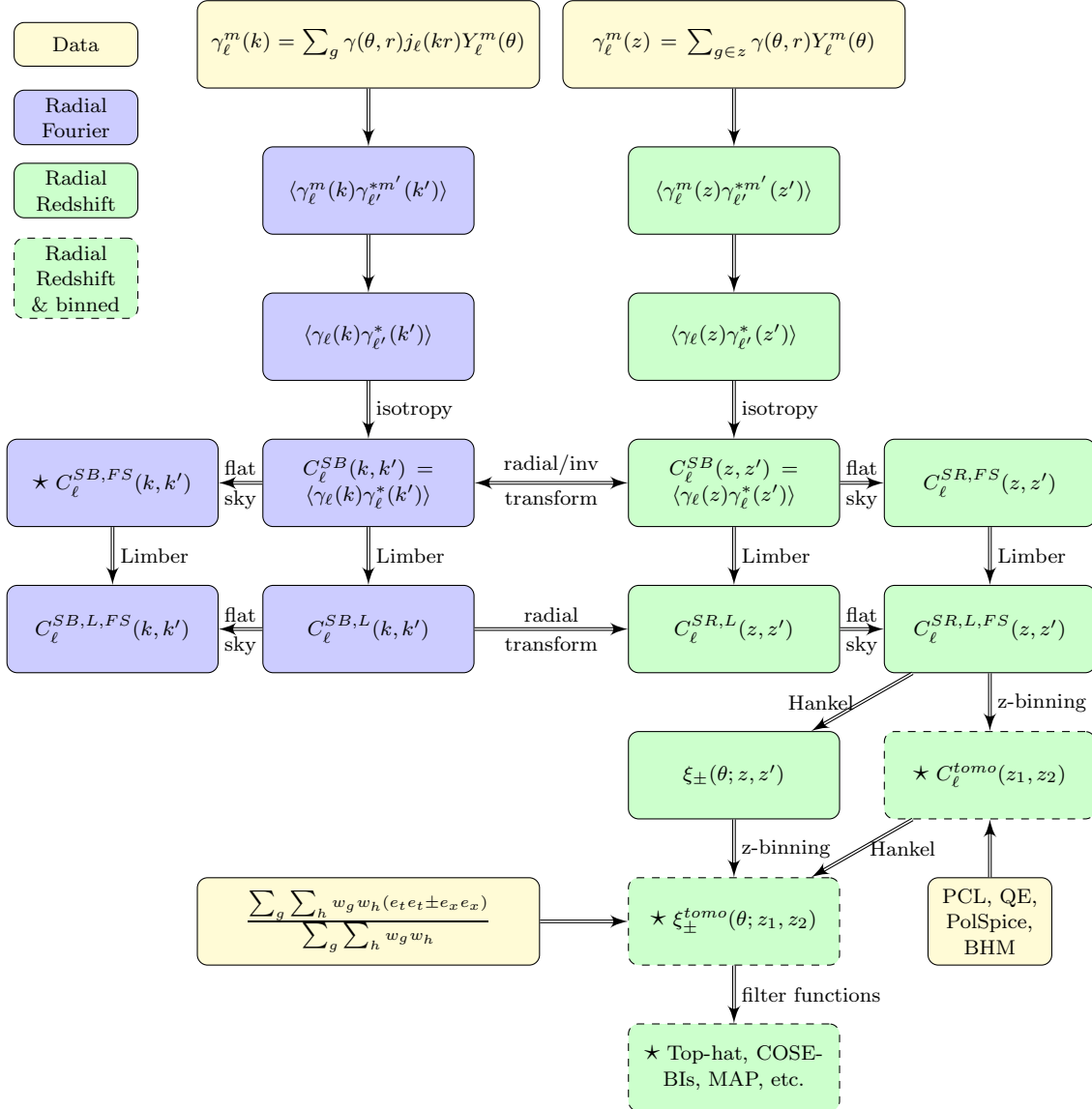


Figure 4. A schema relating each cosmic shear approximation to all others. For brevity we do not include spherical-sky, or non-Limber-approximated Hankel-like transforms (defined in Castro et al., 2005, Section V) as these are not currently in use. Each arrow shows the direction in which a functional approximation or change is applied where the majority of approximations are irreversible. The yellow boxes show places where a statistic can, and has, been approximated from data; these are a direct spherical-Bessel transform (top), a direct correlation function estimator (left), and several power spectrum estimators that are Pseudo- $C(\ell)$ (e.g. Hikage et al., 2011), Quadratic Estimator (Hu & White, 2001), Polspice (The DES Collaboration et al., 2015) and Bayesian Hierarchical Modelling (BHM, e.g. Alsing et al., 2016a,b, Schneider et al., 2016a,b). The blue boxes show statistics that treat the radial (redshift) direction using a Fourier-like/spherical-Bessel analysis, the green boxes show statistics that treat the radial direction directly in redshift space. The solid framed boxes denote full three-dimensional statistics and the dashed framed boxes show redshift binned or ‘tomographic’ statistics. The superscript acronyms SB, SR, FS and L refer to spherical-Bessel, spherical-radial, flat-sky and Limber approximations respectively. Isotropy refers to angular isotropy but not radial, as the shear field probes different look-back times in the expansion history. The labels (k, k') and (z, z') denote continuous scale and redshift variables, and (z_1, z_2) to discretised redshifts. The lower box denoting filter functions refers to Map (e.g. Munshi et al., 2004), COSEBI (Schneider et al. 2010) and top-hat statistics. The stars \star show which statistics have been applied to data.

ponent of Kilbinger et al. (2013) equation 17. This takes into account the full cross-correlation between the ξ_+ and ξ_- statistics. For covariance matrices estimated from simulations, the likelihood is no longer Gaussian and t-distribution should be used (Sellentin & Heavens, 2016), but in this case the covariance matrix is obtained by a mixture of simulated data and analytic terms, and Kilbinger et al. (2013) argue

that the inverse covariance matrix can be used in a Gaussian likelihood.

We find that the overall fit when using the Limber approximation is worse than the full case (larger χ^2 values). The best fit value using the Limber, $T_\ell = 1$ and flat-sky approximations is $\sigma_8 = 0.789 \pm 0.015$ (1- σ) which is consistent with the Kilbinger et al. (2013) values for $\Omega_M = 0.3$,

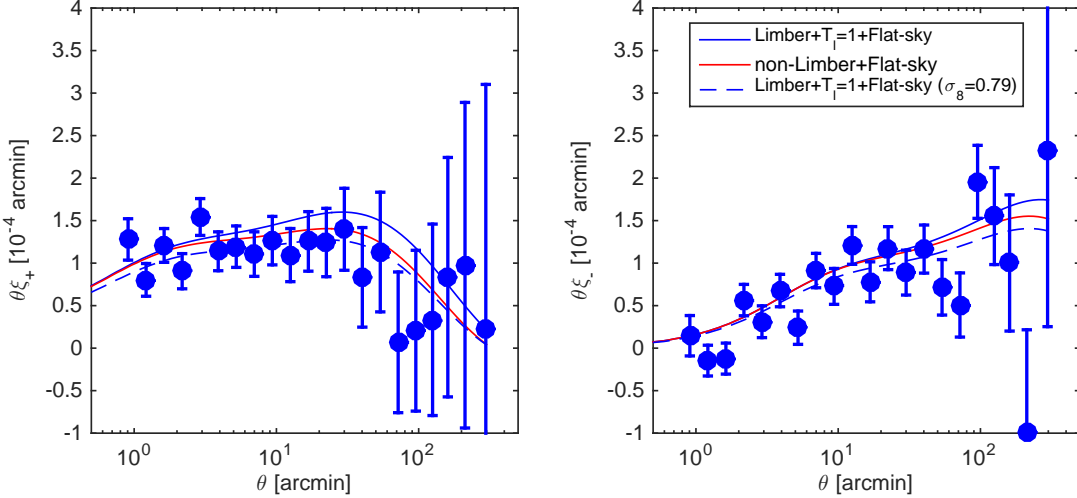


Figure 5. 2D correlation function data from CFHTLenS (Kilbinger et al., 2013). The left panel shows the ξ_+ function and the right hand panel the ξ_- function. The blue lines show the predicted theoretical correlations assuming the Limber approximation for $\sigma_8 = 0.83$ (solid), similar to the *Planck* value, and $\sigma_8 = 0.79$ (dashed), assuming $\Omega_M = 0.3$. The red line shows the predicted correlation functions without using the Limber approximation for $\sigma_8 = 0.83$ assuming $\Omega_M = 0.3$. For plotting the error bars are computed from the inverse diagonal of the full covariance matrices.

Case	$\theta_{\min}/\text{arcmin}$	$\sigma_8 (\Omega_M = 0.3)$	χ^2/dof
Limber+ $T_\ell = 1$ +Flat-sky	0.91	0.789 ± 0.015	1.17
Limber+ $T_\ell = 1$ +Flat-sky, z_{bias}	0.91	0.800 ± 0.017	1.13
Limber	0.91	0.796 ± 0.015	1.12
Limber+ $T_\ell = 1$ +Flat-sky, linear	8.6	0.765 ± 0.023	0.88
Limber+ $T_\ell = 1$ +Flat-sky, linear	17	0.746 ± 0.032	0.89
Full	0.91	0.801 ± 0.016	1.09
Full, z_{bias}	0.91	0.839 ± 0.017	1.06
Full, linear	8.6	0.782 ± 0.023	0.79
Full, linear	17	0.766 ± 0.035	0.82
Planck (2015)	–	0.830 ± 0.015	–

Table 1. The maximum likelihood value of σ_8 (with $\Omega_M = 0.3$) found by fitting the CFHTLenS 2D correlation function data (Kilbinger et al., 2013). We consider the Limber-approximated and non-Limber approximated cases, and the application of the flat-sky approximation. We also show results for two different value of minimum scale used in the analysis, θ_{\min} . Errors shown are $1-\sigma$. The parameter values are also shown in Figure 7. We show reduced χ^2 -values where the degrees of freedom are 42, 26, 20 for $\theta_{\min} = 0.91$, 8.6 and 17' respectively, leading to errors of $\Delta\chi^2 = 0.2, 0.28, 0.32$. We refer to $\theta_{\min} = 8.6$ and 17' as ‘linear’.

who find $\sigma_8(\Omega_M/0.27)^{0.6} = 0.79 \pm 0.03$, and is more than $2-\sigma$ away from the *Planck* (2015) value. For the full case $\sigma_8 = 0.801 \pm 0.016$ ($1-\sigma$), which is a shift of approximately $1-\sigma$ and is well within $1-\sigma$ of the *Planck* maximum likelihood value. In Table 1 we investigate several other cases. In *Planck* (Planck Collaboration et al., 2015) there is a re-analysis of the CFHTLenS Heymans et al., (2013) results where a linear cut in angle is performed with all scales $\theta < 17'$ removed from ξ_+ and all scales from ξ_- . Such cuts are also made in Kilbinger et al. (2013), and in Hildebrandt et al. (2016) removing $\theta < 8.6'$ in ξ_+ . In all these cases the authors found a lower value of σ_8 , which we also find in the Limber-approximated case. However in the non-Limber approximated cases this change is marginally less significant.

In Kitching et al. (2016) a flat-sky spherical-Bessel analysis of the CFHTLenS data was performed and they found that in order for those results to be consistent with *Planck* (2015) a photometric redshift bias similar to that found in

Choi et al. (2015) needed to be included. In Table 1 we show the effect of including the redshift bias from Choi et al. (2015) which has a functional form of $z_{\text{bias}}(z_s) = p_2(z - p_1)$ where $p_2 = -0.19 \pm 0.05$ and $p_1 = 0.45 \pm 0.05$; this is added to the photometric redshift probability distribution in equation (8) as a shift in the mean redshift (see Kitching et al., 2016). We find that when this bias is included $\sigma_8 = 0.829 \pm 0.017$ for the full case, which is in complete agreement with the *Planck* (2015) results. In the Limber, $T_\ell = 1$, and flat-sky approximated case the shift is less pronounced with $\sigma_8 = 0.800 \pm 0.017$ which nevertheless is consistent with the *Planck* (2015) results at $1-\sigma$. Despite this finding we note that the impact of photometric redshift biases on cosmic shear results, and how to propagate these correctly into the statistics, is an open area of investigation. For example Kitching et al., (2016) find $p_1 = 0.26$ and $p_2 = -0.25$ in order for a *Planck* cosmology to be consistent with CFHTLenS; and in Alsing et al. (2016) it was found

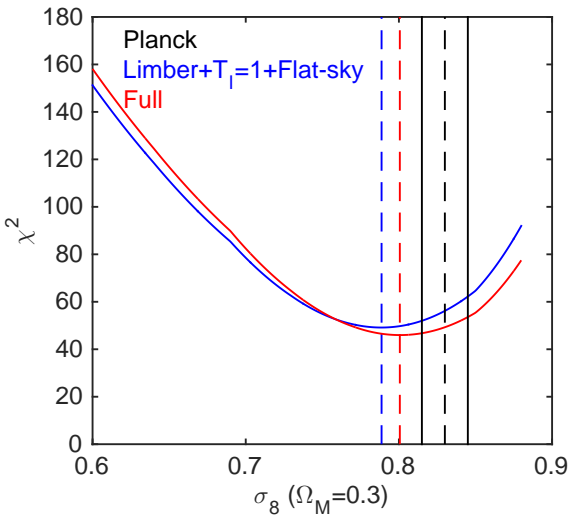


Figure 6. χ^2 fit to the CFHTLenS 2D correlation function data when varying σ_8 , where we assume all other parameters are fixed at the *Planck* maximum likelihood values; including $\Omega_M = 0.3$. We show the χ^2 values for both the Limber, $T_\ell = 1$ and flat-sky approximated case, and the full non-Limber approximated case. The solid curved lines show the goodness of fit, the dashed lines show the best fit values. The black dashed line shows the *Planck* maximum likelihood value, and the solid vertical lines show the $1-\sigma$ error. The number of degree of freedom in the fit is $\text{dof} = 42$.

that assuming a Choi et al. (2015) prior on the photometric bias parameters did not bring about consistency with *Planck*, and a flexible photo-z bias model was not preferred by CFHTLenS alone. Using the KiDS-450 data Joudaki et al. (2016) find that photometric redshift bias correction (using a different approach done by using bootstrap realisations of $n(z)$ given the photometric data) had a statistically insignificant impact on cosmological parameter results.

We note that the DES correlation function results see a similar functional behaviour (a dip at large scales, The DES Collaboration et al., 2015; Figure 1) and also that the KiDS correlation functions also see similar behaviour in the tomographic analysis of that data (Hildebrandt et al., 2016; Figure 5). However we leave a full tomographic re-analysis of these data sets for future work.

4 DISCUSSION

There have been several other investigations into the Limber approximation. For example Giannantonio et al., (2012) concluded that the Limber approximation is accurate for $\ell \gtrsim 20$, however in computing the non-Limber-approximated case a limit of $\ell < kr$ is assumed (see footnote 3 of that paper). Jeong et al. (2009) tested the effect of the Limber approximation on the convergence-convergence power spectra and found a $\sim 1\%$ change in power at $\ell \lesssim 100$, and a 10% change at scales $\ell \lesssim 10$. This result is partly consistent with our analysis where a 10% change in the amplitude of the $C_\ell^{SR}(z, z')$ power spectrum at $\ell \sim 10$ would propagate into ξ_+ and ξ_- statistics with a similar decrease in power on the real-space angular scales presented in current data analyses. However the range of k -modes and redshift ranges

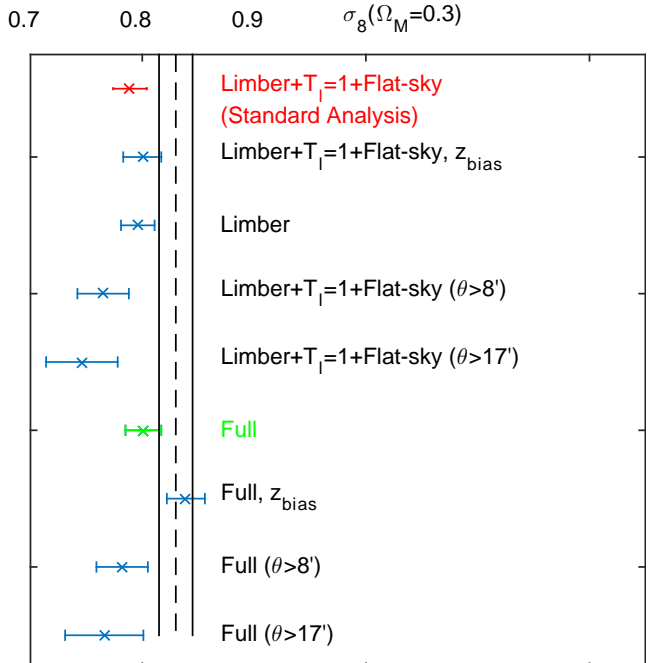


Figure 7. A graphical representation of the results in Table 1. The vertical dashed line is the *Planck* (2015) best-fit value, and the solid lines is the $1-\sigma$ confidence region about this value.

is not quoted in that paper (in particular if a $kr < \ell$ limit is imposed or not) which makes a detailed comparison difficult.

Kitching et al. (2011) applied the LoVerde & Afshordi (2008) approximation (equation 21) in the spherical-Bessel case and compared the case of full (k, z) integration with the $\ell > kr$ case, and found a $\sim 10\%$ change in the amplitude of $C_\ell^{SB}(k, k')$ using the Limber approximation which was approximately constant as a function of ℓ -mode, which is consistent with the results found in this paper. Simon (2007) performed a similar study of the Limber approximation in the galaxy clustering context and found that there is a $\sim 10\%$ bias in the correlation function at scales of $\theta \simeq 260$ arcminutes, which is also consistent with the results found in this paper (see also Section 3.5).

Power spectrum methods, that measure the cosmic shear two-point statistics as a function of ℓ -mode, are more immune to these approximations than correlation function methods because removing $\ell \lesssim 100$ from an analysis will eliminate most of the low- ℓ mode effects. This is the approach taken in Kohlinger et al. (2015) and Alsing et al. (2016b) (both of which made the flat-sky, Limber and tomographic approximations). However a further complication is that the derivative of a Limber-approximated field is not equal to the Limber-approximation of the derivative of the underlying field; this can easily be shown by comparing the functional derivative of the full case with respect to the matter power spectrum, compared to the derivative of the Limber-approximated case. Therefore using a quadratic estimator for a power spectrum (Kohlinger et al., 2015) may have additional difficulties. Power spectrum methods that use a pseudo- $C(l)$, or a mixing matrix method, to account for real-space masks will also encounter additional complexity if the masks mix low- ℓ modes and higher ℓ -modes (e.g. Hikage et al., 2011). Finally super-sample covariance (Takada & Hu,

2013) that causes correlations between the power spectrum errors across ℓ -modes that will also mix low- ℓ and high- ℓ behaviour.

4.1 Validation of Methods on Simulations

In order to test a cosmological likelihood pipeline tests on simulations should be performed where the input cosmology is shown to be recovered, with an accuracy that is consistent with the size of the simulations and the number of simulations in the test set. Such validation tests were shown for example in Kitching et al., (2016) for the spherical-Bessel statistic.

For correlation function analyses validation tests are more complicated for several reasons. In particular simulations are required to estimate the covariance of the statistic. Hildebrandt et al., (2016) and The DES Collaboration et al. (2015) use simulations to determine covariance estimates but do not report validation tests explicitly. Furthermore the covariance estimated on large scales, where the impact of Limber-approximations is expected to be largest, is the most uncertain. For example in a CFHTLenS re-analysis Joudaki et al. (2016) use simulations to test the covariance and show that the uncertainty in the covariance is largest at large scales (Figure 4 of that paper).

Kohlinger et al. (2015) perform validation tests on the CFHTLenS Clone simulations (assuming flat-sky, Limber and tomographic approximations) but note that the large-scales are difficult to recover and that the power is ‘significantly underestimated on large scales’ in the simulations. This can be due to several reasons discussed in Harnois-Deraps & van Waerbeke (2015) where in particular a finite box size in simulations can cause an under-estimation of power, this was also seen in Harnois-Deraps et al. (2012); we also note that this assertion is consistent with the predictions made in this paper. Kiessling et al. (2011) also find a cosmic shear power spectrum from simulations that has a lower amplitude of $\sim 5 - 10\%$ than that predicted from a Limber-approximated tomographic theory, and prescribe this to being due to empty cells in the computation of the power spectrum from those simulations; alternatively this could be due to the effects presented in this paper.

As an alternative to testing on simulations methods have been validated on realisations of random fields, in particular Gaussian random field realisations of cosmic shear power spectra. This approach removes any ambiguity over systematic effects caused by the N-body nature of simulations, however if the random fields are generated as realisations of already approximated cosmic shear power spectra, which was the approach taken Kohlinger et al. (2015) and Alsing et al. (2016b), then any comparison will not fully test the approximations themselves.

In summary validation tests should be performed on simulations however this is complicated for three reasons. First simulations are also required for covariance estimation for some methods, where the uncertainty in the covariance is largest at large scales. Secondly there are degeneracies between the effects predicted in this paper and finite-box effects in simulations which makes a fully consistent validation test more complex. Thirdly tests on Gaussian random fields of cosmic shear power spectra, that make the same assumptions as employed in the data analysis, do not test the

assumptions and approximations themselves. At the current time validation tests on simulations are therefore consistent with the results in this paper, and indeed the predicted suppression on large scales could partly explain some discrepancies between some simulation predictions and theoretical computations.

4.2 Shot Noise Effects

A further consideration is that in general power spectrum estimation may be expected to be more sensitive to shot noise (caused by intrinsic shapes of galaxies; also known as ‘shape noise’) than correlation function analyses. This is because for correlation functions the purely uncorrelated shape noise only enters at zero-lag (zero separation) in the ξ_+ function, and does not enter into the ξ_- function; however second-order effects may enter through coupling of angular scales through the covariance matrix. Whereas a zero-lag effect in angle affects all scales in a power spectrum analysis; manifest as a white noise power spectrum. This is discussed in Mandelbaum et al. (2013) in the context of shape measurement method evaluation. Depending upon the nature of the power spectrum estimation shape noise effects will have a differing effect on results. In Hu & White (2001) they discuss subtraction and marginalisation over the noise power spectrum. In Kohlinger et al. (2015) the estimated noise power spectrum is subtracted from the measurement, and in Alsing et al. (2016) and Kitching et al. (2014) the estimated noise is added to the theoretical modelling. In van Uitert & Schnieder (2016) they propose a position-dependent systematic test for cosmic shear based on correlation function analyses and note a significant excess of signal in their statistic in CFHTLenS at zero-lag. In this analysis we do not include zero separations and so should be more immune to such uncertainties to first order. This will be investigated further in Alsing et al. (in prep).

4.3 CMB Lensing

In Appendix B we also apply the Limber approximation to the case of CMB lensing, and again find that the standard Limber-approximated formulae should be multiplied by a factor of $\ell^4/(\ell + 0.5)^4$. The power spectrum of the convergence is related to the lensing potential power spectrum by $C_\ell^{\kappa\kappa} = [\ell(\ell + 1)]^2 C_\ell^{\phi\phi}$ (Appendix A). These factors have not been accounted for in cross-correlation studies of galaxy weak lensing with other observables, for example Kirk et al. (2016), Harnois-Déraps et al. (2016), Tröster et al. (2016). However for Planck et al. (2016) the Limber-approximated lensing potential power spectrum, derived from a convergence map, and computed using **CAMB** is scaled in the correct way; albeit that the Limber-approximated equations quoted are missing this factor.

5 CONCLUSION

In this paper we present the spherical-Bessel and spherical-radial representations of cosmic shear, and discuss the correlation function representation. We discuss several approximations and limits of these statistics including the flat-sky,

tomographic and Limber approximations. Whilst the tomographic approximation is expected to be relatively benign – because the lensing kernel is relatively smooth in redshift – the flat-sky and Limber approximations change the statistical behaviour of the cosmic shear statistic at large-scales. We also find a subtlety in the derivation of the standard Limber-approximated cosmic shear power spectra formula that neglects an ℓ -dependent factor of

$$T_\ell = \frac{(\ell+2)(\ell+1)\ell(\ell-1)}{(\ell+0.5)^4}, \quad (23)$$

which is equal to unity if the flat-sky approximation is used, and the factor of 0.5 in the denominator is ignored. To include this effect any cosmic shear Limber-approximated $C(\ell)$ should be multiplied by this factor; and in the flat-sky case by $\ell^4/(\ell+0.5)^4$. In general we find that the Limber approximation enhances power on scales $\ell \lesssim 100$, and the flat-sky approximation suppresses power on large scales by $\gtrsim 1\%$ for scales $\ell \lesssim 100$.

We investigate how the angular scales in correlation function analyses map onto ℓ -modes of the cosmic shear power spectrum and find that the following scaling relations are a good fit to the behaviour

$$\begin{aligned} \xi_+ : \log_{10}[\ell_{\max}] &= -0.14 \log_{10}(\theta_{\min}/\text{arcmin}) + 4.06 \\ \xi_- : \log_{10}[\ell_{\max}] &= -0.19 \log_{10}(\theta_{\min}/\text{arcmin}) + 4.49. \end{aligned} \quad (24)$$

We also present mapping between the various cosmic shear statistics used in the literature.

To investigate the impact of the flat-sky and Limber approximations we use the CFHTLenS 2D correlation function data described in Kilbinger et al. (2013). This data, and all cosmic shear results to date, have used tomographic, Limber and flat-sky approximations simultaneously. All results that have used these approximations are also in tension with recent CMB results from Planck (2015). The value of σ_8 from Planck (2015) is 0.83 ± 0.015 which can be compared to Kilbinger et al. (2013) who find $\sigma_8 = 0.79 \pm 0.04$, which is consistent with values found using KiDS data (Hildebrandt et al., 2016) and DES data (The DES Collaboration et al., 2015), DLS (Jee et al., 2015), and other CFHTLenS re-analyses (e.g. Heymans et al., 2012). We find that by not applying the Limber, $T_\ell = 1$ and flat-sky approximations the best-fit value of σ_8 , keeping all other parameters fixed at the Planck (2015) maximum likelihood values, to be $\sigma_8 = 0.801 \pm 0.016$. We also find a better fit to the data where in the Limber, $T_\ell = 1$ and flat-sky approximated case the minimum reduced $\chi^2 = 1.17 \pm 0.2$, and $\chi^2 = 1.09 \pm 0.2$ for the full case.

The only other full-case analysis that has been applied to the CFHTLenS data is from Kitching et al. (2016), who used a flat-sky spherical-Bessel statistic. They found that a small residual bias in photometric redshifts, consistent with those from Choi et al. (2015), were sufficient to result in σ_8 measurements that were in agreement with Planck (2015). We find that adding the residual bias in photometric redshifts from the Choi et al. (2015) paper to the CFHTLenS 2D likelihood results in the full case results in $\sigma_8 = 0.839 \pm 0.017$ which is *a fortiori* consistent with Planck. However the propagation of photometric redshift biases into cosmic shear statistics is an open area of investigation (Alsing et al., 2016b, Hildebrandt et al., 2016; Joudaki et al., 2016).

These results, that have a significant effect on current

surveys will of course be major effects for Euclid, LSST and WFIRST. In this paper we addressed the four most prominent approximations, however there are several further approximations that are expected to have additional impacts on cosmological inference such as source-source clustering (Schneider et al. 2002), source-lens clustering (Bernardeau 1998, Hamana et al. 2002), the Born approximation (Cooray & Hu, 2002), higher-order power spectrum terms (Krause & Hirata, 2010), and unequal-time correlations (Kitching & Heavens, 2016).

When designing cosmic shear statistics extreme care must be taken in choosing which approximations to use, and what limits to impose on the angular and radial wavenumbers used in the analysis. One way of testing assumptions is to validate methods on full simulations that do not make assumptions about the shear field. Another way of alleviating the concerns raised in discovering how sensitive cosmic shear is to these assumptions is to embrace a variety of cosmic shear statistics, where multiple ways of analysing the data should be used in future that will act to test such assumptions and approximations such that the limits of cosmic shear are overcome and the promise of this method is realised for dark energy studies.

Acknowledgements: TDK is supported by Royal Society University Research Fellowship. RJ & LV acknowledge support by Spanish Mineco grant AYA2014-58747-P and MDM-2014-0369 of ICCUB (Unidad de Excelencia ‘Maria de Maeztu’ and Royal Society grant IE140357. JDM is supported in part by the Engineering and Physical Sciences Research Council (grant number EP/M011852/1). The Centre for Computational Astrophysics is supported by the Simons Foundation. We thank the CFHTLenS team for making the correlation function data public. We thank the creators of CAMB for public release of this code. We thank Mark Cropper, Henk Hoekstra, Anthony Lewis, and Paniez Paykari for useful discussions.

REFERENCES

Albrecht, A., Bernstein, G., Cahn, R., et al. 2006, arXiv:astro-ph/0609591

Alsing, J., Heavens, A., Jaffe, A. H., et al. 2016, MNRAS, 455, 4452

Alsing, J., Heavens, A. F., Jaffe, A. H., 2016, arXiv, 1607.00008

Alsing, J., et al., in prep

Battye, R. A., Moss, A., & Pearson, J. A. 2015, JCAP, 4, 048

Bernardeau, F., 1998, A&A, 338, 375

Bridle, S., & King, L. 2007, New Journal of Physics, 9, 444

Brown, M. L., Taylor, A. N., Bacon, D. J., et al. 2003, MNRAS, 341, 100

Castro, P. G., Heavens, A. F., & Kitching, T. D. 2005, PRD, 72, 023516

Choi, A.; et al.; 2016, MNRAS, 463, 2

Cooray, A., & Hu, W. 2002, Astro. Phys. Journal, 574, 19

Dossett J. N., Ishak M., Parkinson D., Davis T., 2015, ArXiv e-prints

Fang, W., Hu, W., & Lewis, A. 2008, Phys. Rev. D, 78, 087303

Fang, W., Wang, S., Hu, W., et al. 2008, Phys. Rev. D, 78, 103509

Fedeli, C. 2014, JCAP, 4, 028

Foreman, S., Becker, M. R., & Wechsler, R. H. 2016, arXiv:1605.09056

Giannantonio, T., Porciani, C., Carron, J., Amara, A., & Pillepich, A. 2012, MNRAS, 422, 2854

Hamana, T., Colombi, S. T., Thion, A., Devriendt, J. E. G. T., Mellier, Y., et al., 2002, MNRAS, 330, 365

Harnois-Déraps, J., Vafaei, S., & Van Waerbeke, L. 2012, MNRAS, 426, 1262

Harnois-Déraps, J., & van Waerbeke, L. 2015, MNRAS, 450, 2857

Harnois-Déraps, J., Tröster, T., Hojjati, A., et al. 2016, MNRAS, 460, 434

Heavens, A. F., 2003, MNRAS, 343, 1327

Heavens, A. F., Kitching, T. D., & Taylor, A. N. 2006, MNRAS, 373, 105

Heavens, A. F., Kitching, T. D., & Verde, L. 2007, MNRAS, 380, 1029

Heymans, C., Brown, M. L., Barden, M., et al. 2005, MNRAS, 361, 160

Heymans, C., Van Waerbeke, L., Miller, L., et al. 2012, MNRAS, 427, 146

Heymans, C., Grocott, E., Heavens, A., et al. 2013, MNRAS, 432, 2433

Hikage, C., Takada, M., Hamana, T., & Spergel, D. 2011, MNRAS, 412, 65

Hildebrandt, H., Viola, M., Heymans, C., et al. 2016, arXiv:1606.05338

Hirata, C. M., & Seljak, U. 2004, Phys. Rev. D, 70, 063526

Hu, W. 1999, Astro. Phys. Journal Letters, 522, L21

Hu, W. 2000, Phys. Rev. D, 62, 043007

Hu, W., & Sawicki, I. 2007, Phys. Rev. D, 76, 064004

Hu, W., & White, M. 2001, Astro. Phys. Journal, 554, 67

Hoekstra, H., & Jain, B. 2008, Annual Review of Nuclear and Particle Science, 58, 99

Jeong, D., Komatsu, E., & Jain, B. 2009, Phys. Rev. D, 80, 123527

Joudaki, S., Blake, C., Heymans, C., et al. 2016, arXiv:1601.05786

Kaiser, N. 1998, Astro. Phys. Journal, 498, 26

Kilbinger, M. 2015, Reports on Progress in Physics, 78, 086901

Kitching, T. D., Heavens, A. F., Taylor, A. N., et al. 2007, MNRAS, 376, 771

Kitching, T. D., Taylor, A. N., & Heavens, A. F. 2008, MNRAS, 389, 173

Kitching, T. D., Heavens, A. F., & Miller, L. 2011, MNRAS, 413, 2923

Kitching, T. D., Heavens, A. F., Alsing, J., et al. 2014, MNRAS, 442, 1326

Kitching T. D; Verde, L; Heavens, A.; Jimenez, R.; 2016, MNRAS, doi: 10.1093/mnras/stw707

Kitching T., & Heavens, A.; 2016, in prep

Kirk, D., Rassat, A., Host, O., & Bridle, S. 2012, MNRAS, 424, 1647

Kirk, D., Omori, Y., Benoit-Lévy, A., et al. 2016, MNRAS, 459, 21

Köhlinger, F., Viola, M., Valkenburg, W., et al. 2016, MNRAS, 456, 1508

Krause, E., & Hirata, C. M. 2010, AAP, 523, A28

Kuijken, K., Heymans, C., Hildebrandt, H., et al. 2015, MNRAS, 454, 3500

Laureijs, R., Amiaux, J., Arduini, S., et al. 2011, arXiv:1110.3193

Leistedt, B., McEwen, J. D., Kitching, T. D., & Peiris, H. V. 2015, Phys. Rev. D, 92, 123010

Limber, N., 1953, ApJ, 117, 134

LSST Science Collaboration, Abell, P. A., Allison, J., et al. 2009, arXiv:0912.0201

Loverde, M., & Afshordi, N. 2008, Phys. Rev. D, 78, 123506

MacCrann, N., Zuntz, J., Bridle, S., Jain, B., & Becker, M. R. 2014, arXiv:1408.4742

Mandelbaum, R., Rowe, B., Bosch, J., et al. 2014, ApJS, 212, 5

Massey, R., Hoekstra, H., Kitching, T., et al. 2013, MNRAS, 429, 661

Mead, A. J., Peacock, J. A., Heymans, C., Joudaki, S., & Heavens, A. F. 2015, MNRAS, 454, 1958

Munshi, D., Valageas, P., & Barber, A. J. 2004, MNRAS, 350, 77

Pan, Z., Knox, L., & White, M. 2014, MNRAS, 445, 2941

Pen, U.-L., Van Waerbeke, L., & Mellier, Y. 2002, Astro. Phys. Journal, 567, 31

Planck Collaboration 2013a, arXiv:1303.5076

Planck Collaboration, Ade, P. A. R., Aghanim, N., et al. 2015, arXiv:1502.01590

Planck Collaboration, Ade, P. A. R., Aghanim, N., et al. 2016, AAP, 594, A15

Sellentin, E.; Heavens, A. F.' 2016, MNRAS, 456, 132

Schneider, P., Eifler, T., & Krause, E. 2010, AAP, 520, A116

Schneider, P., Van Waerbeke, L., Mellier, Y. 2002, A&A, 389, 729

Schneider, M.D., Ng, K.Y., Dawson, W. A., Marshall, P.J., Meyers, J., Bard, D.J., 2016, arXiv:1610.06673

Semboloni, E., Hoekstra, H., Schaye, J., van Daalen, M. P., & McCarthy, I. G. 2011, MNRAS, 417, 2020

Simon, P. 2007, AAP, 473, 711

Smith, R. E., Peacock, J. A., Jenkins, A., et al. 2003, MNRAS, 341, 1311

Spergel, D., Gehrels, N., Baltay, C., et al. 2015, arXiv:1503.03757

Takada, M., & Hu, W. 2013, Phys. Rev. D, 87, 123504

Tegmark, M., Taylor, A. N., & Heavens, A. F. 1997, Astro. Phys. Journal, 480, 22

The Dark Energy Survey Collaboration, Abbott, T., Abdalla, F. B., et al. 2015, arXiv:1507.05552

Tröster, T., Camera, S., Fornasa, M., et al. 2016, arXiv:1611.03554

van Uitert, E., & Schneider, P. 2016, arXiv:1605.01056

APPENDIX A: THE EXTENDED LIMBER APPROXIMATION FOR COSMIC SHEAR

In LoVerde & Afshordi (2008) an extended Limber approximation is presented that was used to assess the accuracy of this approximation as a function of ℓ -mode. Their main result can be captured in the following approximation

$$\lim_{\epsilon \rightarrow 0} \int_0^\infty e^{-\epsilon(x-\nu)} f(x) J_\nu(x) dx = f(\nu) - \frac{1}{2} f''(\nu) - \frac{\nu}{6} f'''(\nu) + \dots \quad (25)$$

where $\nu = \ell + 1/2$, $J_\nu(x)$ are Bessel functions (not spherical), and $f(x)$ is some arbitrary function. Dashes denote derivatives with respect to x . This is then applied to the case of a non-evolving matter power spectrum $P(k)$ (LoVerde & Afshordi, 2008; equation 5) and an extended Limber approximation computed (LoVerde & Afshordi, 2008; equation 11). This calculation however is not strictly appropriate for the cosmic shear case because the matter power spectrum is an evolving field $P(k, z)$.

For cosmic shear we start with equation (5)

$$U_\ell(r[z], k) = \int_0^{r[z]} dr' \frac{F_K(r, r')}{a(r')} j_\ell(kr') P^{1/2}(k, r'), \quad (26)$$

that describes the kernel function for the spherical-Bessel and spherical-radial representations of the cosmic shear field. The integral is along a line-of-sight to a source redshift plane $r[z]$ and encodes the radial transform of the integrated lensing effect caused by perturbations in the matter over-density, that are mapped to the power spectrum via Poissons equation. To make this into a form for which the LoVerde & Afshordi (2008) expansion can be applied we re-write this as

$$U_\ell(r[z], k) = \int_0^\infty dr' w(r[z], r') \frac{F_K(r, r')}{a(r')} j_\ell(kr') P^{1/2}(k, r'), \quad (27)$$

where $w(r, r')$ is a weight function with the following properties: $w(r, r') = 1$ for $r' \leq r$, and $w(r, r') = 0$ for $r' > r$. We can now apply the Limber approximation and find that to first order

$$U_\ell^L(r[z], k) = \left(\frac{\pi}{2\nu k^2} \right)^{1/2} w(r[z], \nu/k) \frac{F_K(r, \nu/k)}{a(\nu/k)} P^{1/2}(k, \nu/k) + \dots \quad (28)$$

where $\nu = \ell + 1/2$; and the pre-factor is a result of the conversion from a spherical Bessel function to a Bessel function. It can be seen explicitly that the weight function is now $w(r, \nu/k) = 1$ for $\nu/k \leq r$, and $w(r, \nu/k) = 0$ for $\nu/k > r$.

The expansion of this case to higher orders can be done using equation (25), however it can be seen that the calculation is more complex than the LoVerde & Afshordi (2008) derivation because the function $f(x)$ in that equation is now $f(r'|r, k) = (\pi/2k^3r)^{1/2}w(r[z], r')[F_K(r, r')/a(r')]P^{1/2}(k, r')$. In particular the expansion does not affect the weight function evaluation $w(r, \nu/k)$ because the arguments to this do not change in the higher order terms. Also the expansion is only valid over the region $\nu/k < r$ where the derivatives of this function are not divergent.

We can now attempt to derive the standard weak lensing formulation of the Limber-approximated cosmic shear power spectrum (Kaiser, 1998) using equations (7) and (8). Substituting equation (28) we find that

$$C_\ell^{SR,L}(z_i, z_j) = |D_\ell|^2 \mathcal{A}^2 \int \frac{dk}{k^2} \int dz_p dz' dz'_p dz'' n(z_p) n(z'_p) p(z_p|z') p(z'_p|z'') W^{SR}(z_i, z_p) W^{SR}(z_j, z'_p) \left(\frac{\pi}{2\nu k^2} \right) \frac{F(r(z'), \nu/k)}{a(\nu/k)} \frac{F(r(z''), \nu/k)}{a(\nu/k)} P(k, \nu/k) \quad (29)$$

where we have absorbed the weight functions w into the integral limits for clarity, and $\mathcal{A} = 3\Omega_M H_0^2/(2\pi c^2)$. To express this equation in the standard form we need to transform integration variables from k to r in the outer integral. This leads to

$$C_\ell^{SR,L}(z, z') = |D_\ell|^2 \mathcal{A}^2 \left(\frac{1}{\nu^4} \right) \left(\frac{\pi}{2} \right) \int dr r^2 \int dz_p dz' dz'_p dz'' n(z_p) n(z'_p) p(z_p|z') p(z'_p|z'') W^{SR}(z_i, z_p) W^{SR}(z_j, z'_p) \frac{F(r(z'), r)}{a(r)} \frac{F(r(z''), r)}{a(r)} P(\nu/r, r), \quad (30)$$

the inner integrals can now be expressed in terms of kernel functions

$$q(r_i, r) = \frac{r}{a(r)} \int dz_p dz' n(z_p) p(z|z_p) W^{SR}(z_i, z_p) \left(\frac{r(z') - r}{r'} \right) \quad (31)$$

where we have expanded the function F_K for the flat-geometry case ($K = 0$). Therefore the Limber-approximated power spectrum can be written as

$$C_\ell^{SR,L}(z, z') = |D_\ell|^2 \mathcal{A}^2 \left(\frac{1}{\nu^4} \right) \left(\frac{\pi}{2} \right) \int dr q(r_i, r) q(r_j, r) P(\nu/r, r). \quad (32)$$

This is the standard form for the cosmic shear power spectrum (see e.g. Hu, 1999; Joachimi & Bridle, 2009), except that the ℓ -dependent pre-factor is different. The full ℓ -mode dependent prefactor is

$$T_\ell = \frac{|D_\ell|^2}{\nu^4} = \frac{(\ell+2)(\ell+1)\ell(\ell-1)}{(\ell+0.5)^4}. \quad (33)$$

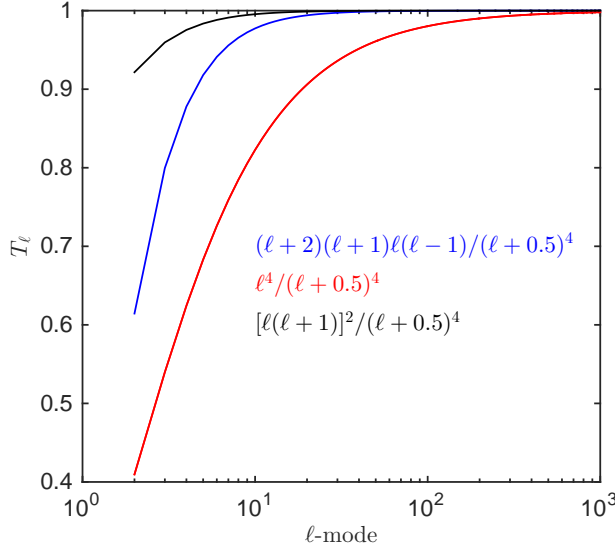


Figure 8. The functional form of the ℓ -dependent prefactor in equations (32), (33) and (34), for the cosmic shear spherical (blue) and flat-sky (red) cases, and for the convergence case (black).

In the standard derivation there are two assumptions that remove this pre-factor. These assumptions are the flat-sky approximation whereby $|D_\ell|^2 = \ell^4$, and the approximation $\nu = \ell$ (or $\ell = (\ell + 0.5)$). In this case $T_\ell = 1$ and the standard result is recovered. However these approximations can have a large impact on the amplitude of the power spectrum at $\ell \lesssim 100$ as we investigate in this paper. In Figure 8 we show the functional form of T_ℓ . To recover the correct ℓ -mode scaling from a standard cosmic shear analysis one should multiply by T_ℓ .

One can also compute a convergence power spectrum from weak lensing data. This is different from the shear case only in that the factor $D_\ell = \ell(\ell + 1)$ in the spherical-sky case. Following the derivation above we find that the Limber-approximated convergence power spectrum is the same as equation (32) but with an ℓ -dependent prefactor of

$$T_\ell^\kappa = \frac{[\ell(\ell + 1)]^2}{(\ell + 0.5)^4}. \quad (34)$$

Again, under the assumption that $\nu = \ell$ and $\ell \simeq \ell + 1$ this factor cancels, but does not in general. We again show the effect in Figure 8, which is less pronounced than for the shear case.

APPENDIX B: CMB LENSING CASE

The derivations of Appendix A can also be applied to the power spectrum of the lensing potential as probed by CMB lensing. This can be written as (Kitching, Heavens, Das, 2011)

$$C_\ell^{\phi\phi} = \mathcal{A}^2 \int \frac{dk}{k^2} G_\ell(k) G_\ell(k) \quad (35)$$

where $\mathcal{A} = 3\Omega_M H_0^2/\pi c^2$, k is a radial wavenumber and

$$G_\ell(k) = \int_0^{r[z_{\text{CMB}}]} dr' \frac{F_K(r[z_{\text{CMB}}], r')}{a(r)} j_\ell(kr') P^{1/2}(k, r'), \quad (36)$$

where $r[z_{\text{CMB}}]$ is the comoving distance to the surface of last scattering, $F_K(r, r') = (r - r')/rr'$ in a flat geometry, $a(r)$ is the dimensionless scale factor, $j_\ell(kr)$ are spherical Bessel functions of the first kind, and $P(k, r)$ is the power spectrum of matter overdensities.

We can now apply the Limber approximation in the same way as Appendix A and find that to first order

$$G_\ell^L(k) = \left(\frac{\pi}{2\nu k^2} \right)^{1/2} w(r[z_{\text{CMB}}], \nu/k) \frac{F_K(r[z_{\text{CMB}}], \nu/k)}{a(\nu/k)} P^{1/2}(k, \nu/k) + \dots \quad (37)$$

where $\nu = \ell + 1/2$; and the pre-factor is a result of the conversion from a spherical Bessel function to a Bessel function. $w(r, r')$ is a weight function with the following properties: $w(r, r') = 1$ for $r' \leq r$, and $w(r, r') = 0$ for $r' > r$.

Substituting this into the expression for $C_\ell^{\phi\phi}$ we find that

$$C_\ell^{\phi\phi} = \mathcal{A}^2 \frac{\pi}{2\nu} \int \frac{dk}{k^4} \frac{P(k, \nu/k)}{a(\nu/k)} \left[1 - \frac{\nu/k}{r[z_{\text{CMB}}]} \right] \quad (38)$$

where we assume that the weight function w is absorbed into k integral limits. We can convert to an integral over r through a change of variables such that

$$C_\ell^{\phi\phi} = \mathcal{A}^2 \frac{\pi}{2\nu^4} \int dr r^2 \frac{P(\nu/r, r)}{a(r)} \left[1 - \frac{r}{r[z_{\text{CMB}}]} \right]. \quad (39)$$

This again differs from the standard expression (Pan et al., 2014; Planck et al., 2016) by a factor of $\ell^4/(\ell + 0.5)^4$.